RESONANCE ION DISSOCIATION SPECTROSCOPY OF CH_3I^+ PRODUCED BY MOLECULAR BEAM ELECTRON-IMPACT IONIZATION

J.A. SYAGE, J.E. POLLARD and J. STEADMAN [1]

Aerophysics Laboratory, The Aerospace Corporation, P.O. Box 92957, Los Angeles, CA 90009, USA

Received 16 June 1989; in final form 12 July 1989

A new approach for recording high resolution spectra of cold nonfluorescing polyatomic ions is demonstrated. Electron-impact ionization of jet-cooled polyatomic molecules produces parent ions with nearly the same rotational temperature as that of the neutral beam and a vibrational distribution dominated in many cases by diagonal Franck–Condon factors. Resonant laser photodissociation of the cold parent ion followed by mass selective detection of the photofragment then leads to highly resolved vibronic spectra. We demonstrate the experimental capability using the $\tilde{A}\leftarrow\tilde{X}\,^2\Pi_{1/2}$ transition of CH_3I^+ as an example. In addition, the unexpected absence of the umbrella mode $\nu_2(1, 1)$ transition is explained.

1. Introduction

High resolution spectroscopy of gas phase polyatomic ions poses many experimental challenges due to spectral congestion from thermal rovibrational distributions, quenching of emission by rapid radiationless decay or dissociation, and the relatively low ion densities achievable by conventional means. Consequently, spectroscopic information of polyatomic ions (greater than three atoms) is very limited. In this paper we describe a new technique based on molecular beam electron-impact (EI) ionization and resonance ion dissociation (RID) and compare it to other recent RID spectroscopic developments.

The field of ion spectroscopy has been extensively reviewed, and a comparison of different high resolution techniques can be found in refs. [1–3]. Ion photodissociation spectroscopy has an extensive history of use in ion beam [4] and ion cyclotron resonance (ICR) spectrometers [5]. These techniques typically generate ions by discharges or by EI of thermal samples, which often results in spectral congestion. Ion beam studies usually focus on diatomic and triatomic ions that permit the recording of highly resolved spectra despite the broad distribution of internal energies. The spectra of large ions, which are usually the subject of ICR studies, usually show poorly resolved vibrational structure.

Recent efforts to produce cold polyatomic ions have relied on molecular beam methods. Woodward et al. took advantage of threshold resonance-enhanced multiphoton ionization (REMPI) in molecular beams to create cold CH_3I^+ ions for recording single-photon photodissociation spectra [6]. Syage and Wessel similarly used threshold REMPI to form cold naphthalene ions in a molecular beam, but used multiphoton absorption to record RID spectra [7]. Multiphoton ion dissociation methods were further developed by Schlag and coworkers [8], and Ripoche et al. [9]. All of these studies had in common the use of two independently tunable dye lasers, one to ionize the molecules and the other to photodissociate the ions.

EI ionization in free-jet expansion has been used to form cold parent ions that were detected by emission spectroscopy [10,11]. In this paper, we extend the idea to molecular beam mass spectrometry to achieve high resolution RID spectroscopy of nonfluorescing ions in a single-laser experiment. The crossed electron–laser–molecular beam method yields spectral resolution comparable to the two-laser experiments, but is simpler, more economical, and less restrictive in the choice of precursors for forming cold ions. The two-laser molecular beam ion photodis-

[1] National Research Council Postdoctoral Associate.

0 009-2614/89/$ 03.50 © Elsevier Science Publishers B.V.
(North-Holland Physics Publishing Division)

sociation experiments of CH_3I^+ by Woodward et al. [6] and Schlag and coworkers [8] serve as good examples of high resolution electronic state spectroscopy of a polyatomic ion. We have therefore chosen for the present work the $\tilde{A}\leftarrow\tilde{X}\,^2\Pi_{1/2}$ transition of CH_3I^+, to enable a comparison with the two-laser RID spectra.

2. Experimental

The molecular beam time-of-flight (TOF) mass spectrometer consists of differentially pumped source and ionization chambers. Aside from the pulsed electron beam source, it is of conventional design and is described in greater detail elsewhere [12,13]. Typical pulsed expansion conditions were 5% CH_3I in 25 psia Ar, 500 μm nozzle diameter, 20 mm nozzle–skimmer distance, and 400 μs pulse width. The ambient base pressure in the ionization chamber is typically 3×10^{-8} Torr, rising to about 2×10^{-7} Torr during operation of the pulsed nozzle at 10 Hz.

The pulsed EI ion source, shown in fig. 1a, is a slightly modified version [13] of the design by Pollard and Cohen [14]. Electrons are generated by thermionic emission from a hot tungsten hairpin filament. The bias voltage V4 applied to the filament determines the electron beam energy. The electron pulse is admitted to the field-free excitation region by applying to V3 a gate pulse P3 (duration 200–400 ns). The electron beam is collimated to a diameter of approximately 5 mm by the apertures at V2 and V3. This ensures complete overlap with the molecular beam. The excitation region is maintained field free during the electron beam pulse by applying a constant (1500 V) potential to grids V1 and V2. The ions formed are then accelerated into the TOF mass spectrometer by applying to V2 a 75 V repeller pulse P2 (duration 5 μs). Although the electron beam points in the direction of the detector, electrons are prevented from reaching the detector by the negative potential gradient (field) from V1 to V0. The EI source was designed for narrow electron energy distributions (by using a hairpin filament) rather than for large fluxes. Consequently, the ionization efficiency is only about 10^{-6}.

The discrimination of photofragment ions from primary fragment ions formed in the ionization step was achieved by two methods. The first method was adapted from Woodward et al. [6], except that the photodissociation laser pulse was delayed with respect to the onset of the repeller pulse as portrayed in fig. 1b. The photofragment ions therefore arrive at the detector after the primary fragment ions. The delay time ($\approx$400 ns) was adjusted so that the desired photofragment ion signal was sufficiently sep-

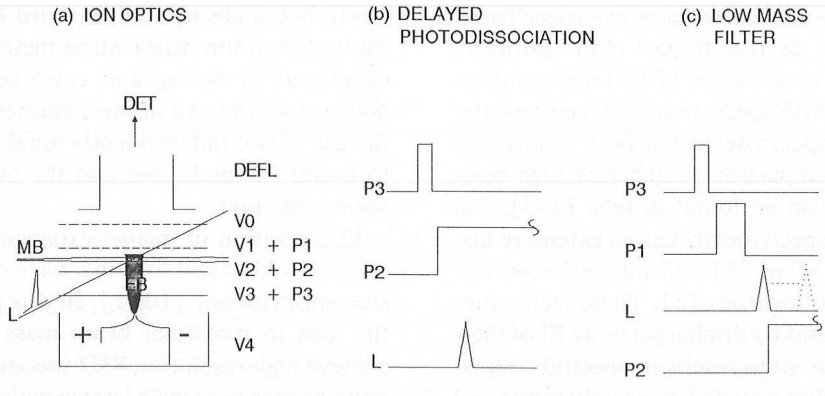

Fig. 1. (a) Crossed electron–laser–molecular beam ion optics assembly. The electron beam (EB) is activated by applying a gate pulse P3 to V3, and the ions are then extracted by applying a pulse P2 to V2. Deflector plates (DEFL) are used to compensate for ion drift resulting from the molecular beam (MB) velocity. (b) The laser pulse (L) is delayed with respect to P2 giving rise to a corresponding delay between photofragments and primary ions of the same mass. (c) In this arrangement, the primary ions are first accelerated away from the detector by P1+V1 and then reversed by dropping P1 and activating P2. Lighter ions that have traveled past the V2 grid are not detected.

arated from the strong primary signal and did not overlap with other weaker primary ion mass signals. The second method, illustrated in fig. 1c, is based on a new but simple concept that will be described in greater detail elsewhere [15]. The traditional three-grid Wiley and McLaren ion optics [16] is operated as a low mass rejection filter in which pulse P1 is applied to V1 to create a reverse bias that causes the initially formed primary ions to travel away from the detector. The P1 voltage and duration define a cutoff point for light masses which exit the lower V2 grid. A positive bias is then applied by turning on P2. A TOF mass spectrum of only the heavier masses results. If a photodissociation laser pulse is applied subsequent to the low mass filtering period, then photofragment ions appear in the mass spectrum against a zero background. This method is similar in concept but different in approach from the reflectron energy filtering used by Schlag and coworkers [8].

The electron beam an repeller pulses, P3 and P2, were synchronized with the laser pulse either by using the variable delay Q-switch sync-out pulse from the photodissociation laser to trigger the P3 and P2 pulse generators, or by using a master pulse generator to externally Q-switch the laser and the P3 and P2 pulse generators. The latter arrangement allowed a greater range of relative delay between P2 and the laser pulse. The laser pulses (about 5 ns and 40 mJ or less) entered the chamber either unfocused or defocused so that the beam diameter ($\approx$4 mm) enveloped the intersection of the molecular and electron beam. The spectra presented here were normalized to laser intensity and represent single traces at a scan rate of about 0.12 nm/min, a pulse repetition rate of 10 Hz, and an effective integrating constant of about 0.05 nm.

3. Results and discussion

3.1. Ion photodissociation detection sensitivity

A common problem in ion photodissociation experiments is distinguishing between fragments formed during ionization from those formed by ion photodissociation. In previous studies of CH_3I^+, it was necessary to delay the ionization and dissociation pulses to separate in time the CH_3^+ produced in each step. Woodward [6] relied on the different arrival times at the detector in monitoring the photodissociated CH_3^+. Schlag and coworkers [8] refined the selectivity by applying a voltage pulse between the two laser pulses and using a reflecting electric field filter adjusted to eliminate the higher energy CH_3^+ fragments formed by the first laser. In both cases the delay times were sufficiently large to require independently pumped dye lasers.

The effectiveness of our methods for separating the primary CH_3^+ signal from the photofragment ion signal is shown by the series of mass spectra in fig. 2. The complete EI/TOF mass spectrum is shown without laser photodissociation. Fig. 2a shows an expanded region of the EI mass spectrum, consisting of the ionization fragment CH_3^+ and Ar^{2+} (mass/charge ratios of 15 and 20, respectively). By using delayed photodissociation, the CH_3^+ photofragment signal occurs at later time relative to the primary CH_3^+, as shown in fig. 2b. By adjusting the time de-

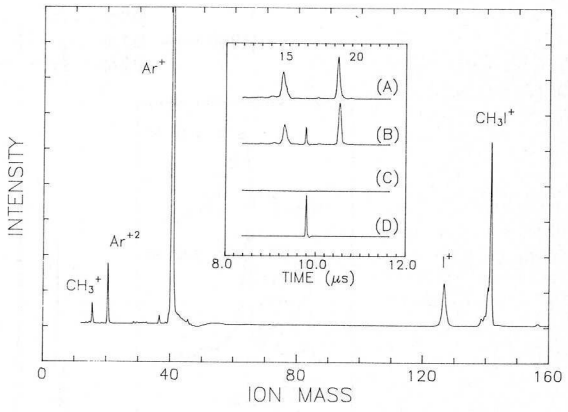

Fig. 2. EI/TOF mass spectra of CH_3I. Insert shows the effect of selective detection of photofragment ions by the two methods portrayed in fig. 1. (a) Conventional EI/TOF mass spectrum (no laser). Primary CH_3^+ and Ar^{2+} are denoted by their mass/charge ratios of 15 and 20, respectively. (b) Same as (a), but with time delayed photodissociation laser pulse giving rise to a corresponding delay between the primary and photofragment CH_3^+ signals. (c) EI/TOF mass spectrum with low mass rejection filter (no laser). (d) Same as (c), but with photodissociation laser pulse creating CH_3^+ photofragment. Conditions were 60 eV EI energy, $\lambda = 576.37$ nm, and 30 mJ/pulse unfocused.

lay the photofragment signal is positioned so that it does not overlap with either primary CH_3^+ or background ion signals other than CH_3^+. Even more effective for mass discrimination is the low mass rejection filter technique by which primary ion signals below a prescribed mass are eliminated before the photodissociation pulse arrives. As shown in fig. 2c in the absence of a photodissociation pulse, all lower masses are rejected. In the presence of the photodissociation pulse, the photofragment CH_3^+ signal is observed against a zero background (fig. 2d). We estimate the sensitivity of detecting ion photodissociation as follows: A molecular beam density of $\approx 10^{13}$ cm^{-3} for a 5% mixture of CH_3I in Ar, and an EI ionization efficiency of 10^{-6} produces a CH_3I^+ density of $\approx 5\times 10^5$ cm^{-3}. (This figure ignores dilution due to dissociative ionization and excitation to other electronic states of CH_3I^+ that do not participate in the $\tilde{A}\leftarrow\tilde{X}\,^2\Pi_{1/2}$ transition of interest.) Resonant dissociation of CH_3I^+ results in a mass spectrum for the delayed photofragment CH_3^+ with a signal-to-noise ratio (with 100 pulse averaging) of $\geqslant 100$ and $\geqslant 30$, with and without low mass filtering, respectively. This corresponds to photodissociation detection sensitivity on the order of 10^3–10^4 cm^{-3}. This excellent detection limit is partly due to the large ionization volume defined by the intersection of the electron and molecular beams.

3.2. Rotational cooling

The primary objective of this work is to demonstrate that cold ion RID spectroscopy, free of the usual problems associated with interference from primary ion signals, can be achieved in a single-laser experiment by using EI ionization in a jet-cooled sample. An ample demonstration of this is given by the recorded $\tilde{A}\leftarrow\tilde{X}\,^2\Pi_{1/2}$ transition of CH_3I^+ in the one-photon dissociation region shown in fig. 3. Examples of our rotational bandshapes are plotted in figs. 3 (insert) and 4, and represent features that were emphasized in the two-laser molecular beam work of Woodward et al. [6] and Schlag and coworkers [8]. The expansion of CH_3I in 25 psi Ar leads to substantially better rotational cooling than the expansion in neat CH_3I (fig. 4). The range of EI energy

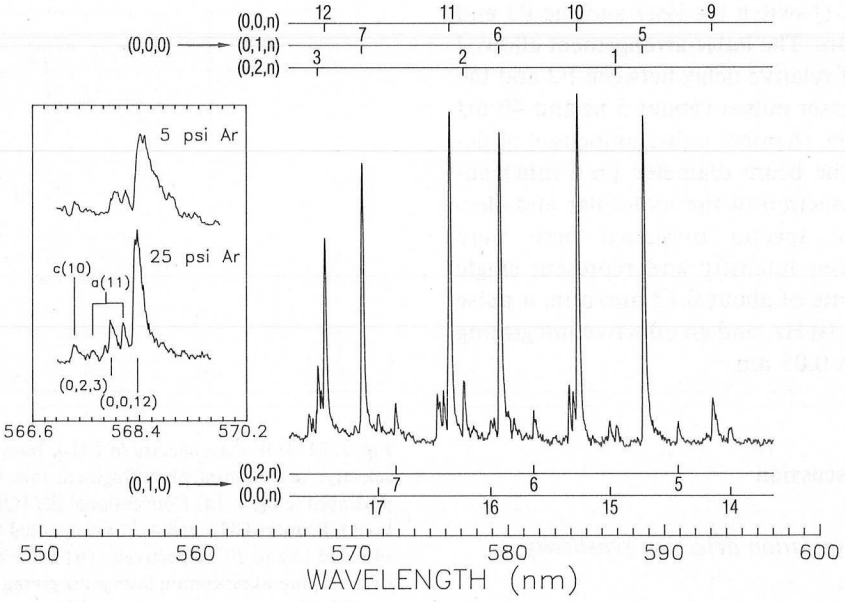

Fig. 3. One-photon RID spectrum of the $\tilde{A}\leftarrow\tilde{X}\,^2\Pi_{1/2}$ transition of CH_3I^+. The assigned transitions are from ref. [8], where (ν_1, ν_2, ν_3) corresponds to the symmetric modes, C–H stretch, umbrella, and C–I stretch, respectively. The lower set of assignments represent transitions from vibrationally excited ν_2. The designations $a(n)$ and $c(n)$ in the insert refer to unassigned progression first reported in ref. [8].

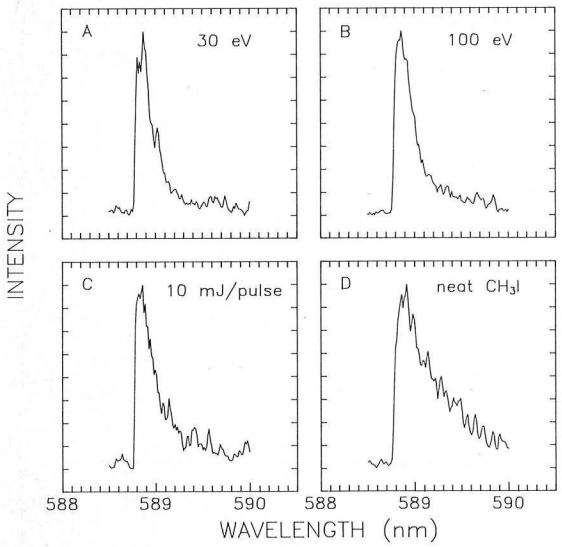

Fig. 4. Rotational contours of the $(0, 0, 0) \rightarrow (0, 1, 5)$ line. Conditions were 5% CH_3I in 25 psi Ar, 60 eV ionization and 30 mJ/pulse ($\approx 1 \times 10^7$ W/cm^2), unless otherwise stated. The bandshapes under the conditions in fig. 3 were essentially identical to (a) and (b).

(20–100 eV) (figs. 3, 4a and 4b) and laser flux ($\leqslant 10^7$ W/cm^2) (figs. 3 and 4) employed in these studies are also shown not to contribute noticeably to the linewidths. The RID linewidths measured in this work (e.g. figs. 4a, 4b and 4c) were typically 6 cm^{-1}, which is about the same as that observed using molecular beam REMPI ion production [6,8]. Because the rotational constants of the $\tilde{X}$ and $\tilde{A}$ states are not accurately known (as far as we know), we cannot calculate the ion rotational temperature from the rotational contours. However, the RID linewidths by molecular beam EI ionization are substantially narrower than the 60–70 cm^{-1} widths observed by Morrison and coworkers [17] using EI ionization of a thermal sample of CH_3I. Clearly, the jet-cooled rotational temperature of the neutral CH_3I is effectively preserved in the EI ionization.

Prior studies of rotational excitation by EI indicate that the excitation process is reasonably well approximated by one-photon electric-dipole selection rules (i.e. $\Delta J = \pm 1$), with small deviations from pure dipole behavior becoming pronounced for decreasing EI energies [18,19]. These deviations, presumably due to multipolar contributions, account for weak $\Delta J > 1$ transitions. For molecules with large rotational constants (e.g., diatomics), increases of just a few rotational quanta correspond to moderate rotational heating. This concern has been raised [19] in applications where the rotational distribution from EI dispersed fluorescence spectra of electronically excited ions is used as a measure of the rotational distribution in the precursor neutral (EI thermometry [20]). For the frequently studied case of N_2, the rotational heating due to EI ionization can be as much as 50 K [19]. The extent of rotational heating due to $\Delta J > 1$ transitions, however, is greatly diminished for larger polyatomic ions because of their smaller rotational constants. This accounts for the narrow linewidths observed in this work. Similar conclusions have been reached by Maier and coworkers in the spectroscopy of fluorescing ions formed by EI in a free jet [10].

3.3. Vibrational distribution

The spectrum in fig. 3 is essentially free of hot band structure that would result from vibrational excitation in the EI ionization process. Only the minor presence of the $\nu_2^+ = 1$ hot band series is apparent in fig. 3. Because electron excitation is fairly well approximated by electric-dipole selection rules [18,19], vibrational excitation in the ion will depend on the Franck–Condon (FC) factors $\langle \nu_m | \nu_m^+ \rangle$ connecting the vibrational levels between the neutral ground electronic state and the ion electronic state(s), where, ν designates the vibrational mode, m denotes the vibrational quantum number, and the superscript + refers to ion states. The ratio of the transition probabilities for vibrationless and vibrational-ion excitation can be expressed by

$$P(0_0^+)/P(\nu_m^+) = |\langle \nu_m | 0_0^+ \rangle|^2 / |\langle \nu_m | \nu_m^+ \rangle|^2 .$$

This ratio is maximized for vibrationless neutral molecules (i.e. $\nu_m = 0_0$) and small geometry changes. The former condition is effectively achieved in a supersonic expansion. The latter condition cannot, of course, be controlled. However, even for moderate geometry changes, FC calculations show that the probability of forming vibrationless ions is greatest when the precursor neutral molecules are vibrationless. Consequently, unless the ion geometry is quite different from the neutral geometry (e.g. NH_3), then

it is reasonable to expect that the vibrationless transition probability will dominate in molecular beam ionization. Single-photon photoelectron spectra [21] can serve as a guide for choosing favorable molecules on the basis of ion vibrational excitation.

Finally, we comment on the surprising absence of the $(0, 1, 0)\rightarrow(0, 1, n)$ hot band progression (fig. 3). These missing features are intriguing because of the presence of the $(0, 1, 0)\rightarrow(0, 0, n)$ and $(0, 2, n)$ progressions, as well as the strong $\Delta\nu_2^+ = 0$ progression that occurs the vibrationless $\tilde{X}(0, 0, 0)$ level. This unusual effect in CH_3I^+ was first reported without explanation as an "anomaly" by Woodward et al. [6]. Their REMPI work involved the specific preparation of the (0, 1, 0) vibrational level in the spin–orbit split ground electronic states $\tilde{X}\,^2\Pi_{1/2}$ and $\tilde{X}\,^2\Pi_{3/2}$, thus accentuating the effect observed in the weak hot band transitions in fig. 3. The missing $(0, 1, 0)\rightarrow(0, 1, n)$ progression can be explained by a negligible Franck–Condon (FC) overlap for the $\nu_2^+(1, 1)$ transition (henceforth 2_1^1). This can occur in electronic transitions in which the vibrational potential energy surfaces are of similar shape, but are shifted in their equilibrium position to an extent that the vibrational wavefunctions are nearly exactly out of phase (i.e. destructive interference).

We have calculated FC factors $R(m, n)$ for ν_2^+ transitions (denoted as 2_m^n) using a displaced harmonic oscillator model [22]. The dependence of $R(m, n)$ on geometry change is represented by a geometric distortion parameter γ along the normal coordinate, defined by

$$\gamma = -\alpha' d\,[\beta/(1+\beta)]^{1/2},$$

$$\beta = \alpha''/\alpha' = \nu''/\nu', \quad \alpha^2 = 4\pi^2\nu/h.$$

The labels m and $''$, and n and $'$ refer to the ground and excited ion states $\tilde{X}$ and $\tilde{A}$, respectively. The term d is the change in the vibrational normal coordinate upon electronic excitation (i.e. $d = q' - q''$) and is defined such that αd and, therefore, γ are dimensionless quantities. For two similarly shaped harmonic potentials (i.e. $\nu' \approx \nu''$), a value of $\gamma = 1$ corresponds to a displacement of about 1/4 of the width of the potential at $\nu = 1$.

Calculated spectral intensities (proportional to $R(m, n)^2$) are presented in fig. 5 for the 2_0^n and 2_1^n transitions as a function of γ. These results distinctly show that the 2_1^1 transition vanishes at a value

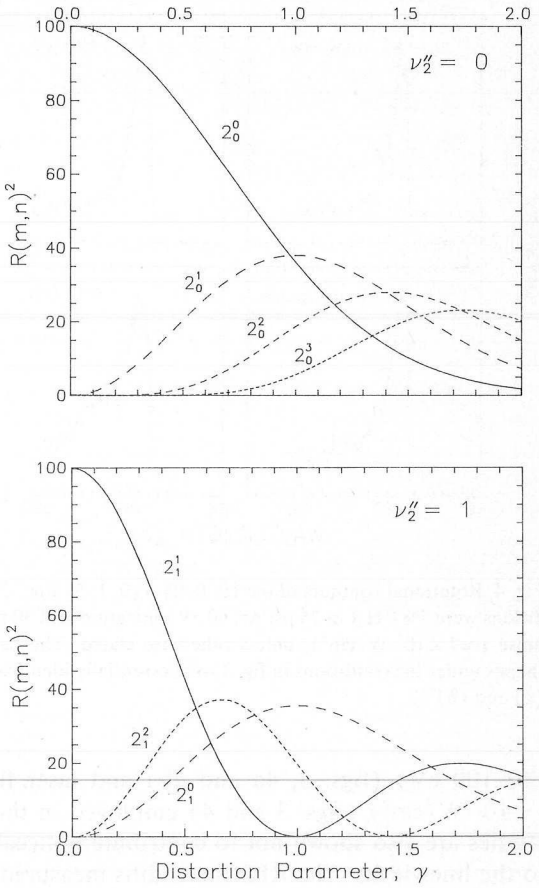

Fig. 5. Calculated distribution for the 2_0^n and 2_1^n FC progression. The parameter γ is proportional to the change in the ν_2 equilibrium coordinate for the $\tilde{A}\leftarrow\tilde{X}\,^2\Pi_{1/2}$ transition. Calculations assume $\nu_2'' = 1245\ cm^{-1}$ and $\nu_2' = 1204\ cm^{-1}$ [6].

of $\gamma = 1.0$. This measure of the geometry change is also consistent with the other observed 2_m^n transition intensities. Because 2_m^n forms strong combinations with the ν_3 progression (i.e. $2_m^n 3_0^n$), a discussion of relative intensities is difficult. The region of the spectrum reported by Woodward et al. includes the $2_1^0 3_0^n$ $(n = 5–7)$ and $2_1^2 3_0^n$ $(n = 14–16)$ transitions. (Fig. 3 covers a slightly larger spectral region, showing the $n = 17$ line for the latter progression.) Unfortunately, the two series do not have a common value of n in which to compare relative intensities. However, by using the measured (but qualitative) 3_0^n intensity distribution [8] as a weighting factor, one obtains an intensity ratio for $2_1^0/2_1^2$ of about 1.4,

which is in excellent agreement with calculations for $\gamma = 1$ (fig. 5).

The vibrationless progression 2_0^n, in combination with 3_0^n (fig. 3), has been more extensively studied. From ref. [8], it was possible to obtain the following approximate relative intensities: $2_0^1 3_0^n / 2_0^0 3_0^n = 0.96$ (averaged over $n = 10$–16) and $2_0^2 3_0^n / 2_0^1 3_0^n = 0.92$ (averaged over $n = 8$–13). Again, within the uncertainty of this estimation, the relative intensity distribution is in accord with the calculations for $\gamma = 1.0$ (fig. 5). It is worth noting that FC interference effects (e.g. the missing 2_1^1 progression) can enable a more precise determination of γ than would be possible on the basis of the relative intensity analysis (e.g. that discussed above). Because FC interference occurs only for vibrational wavefunctions exhibiting nodes, a study of transitions involving vibrationally excited ions (e.g. hot bands) can be very informative.

4. Conclusions

This work has demonstrated that EI ionization of precursor molecules cooled in a supersonic molecular beam is a versatile method for preparing cold polyatomic ions for high resolution RID spectroscopy. It should be noted that only parent ions will be cold, however, we have found that at moderate energy (20–100 eV), EI excitation of jet-cooled molecules nearly always produces a sufficient yield of parent ions for photodissociation studies. It has been suggested in previous work [6] that the ion rotational distribution can be reduced even further by using narrowband REMPI excitation to select a subset of the neutral rotational distribution. In our findings, however, the RID linewidths from EI ion production were less than or equal to those observed in spectra [6,8] that relied on REMPI ion production. REMPI holds an advantage over EI ionization if specific vibrational excitation in ions is desired [6,7], however, for rotational cooling, and in many cases vibrationless ionization, the two methods are comparable.

The EI molecular beam method is not without its limitations. The ionization efficiency is much less than by MPI, although, the larger ionization volume compensates for this deficiency. The larger ionization volume, on the other hand, makes multiphoton dissociation studies more difficult. On the whole, though, EI molecular beam ionization has some clear advantages over REMPI as a source of cold ions. Aside from the simplicity and economy of dispensing with the ionization laser, the method is very general in that essentially *any* molecule may be used as a precursor for producing rotationally cold parent ions. REMPI excitation requires molecular energy level structures that meet stringent intermediate state and ionization threshold conditions, and is therefore limited in the choice of candidate ions.

Acknowledgement

We gratefully acknowledge discussions with John Wessel and software assistance from Eric Fournier. This work was supported by the Aerospace Sponsored Research program.

References

[1] T.A. Miller and V.E. Bondybey, eds., Molecular ions: spectroscopy, structure and chemistry (North-Holland, Amsterdam, 1983).
[2] J.P. Maier, ed., Ion and cluster ion spectroscopy and structure (Elsevier, Amsterdam, 1989).
[3] J.A. Syage and J.E. Wessel, Appl. Spectros. Rev. 24 (1988) 1.
[4] J.T. Moseley, Advan. Chem. Phys. 40 (1985) 245.
[5] R.C. Dunbar, in: Ionic processes in the gas phase, ed. M.A. Almoster Ferreira (Reidel, Dordrecht, 1984).
[6] A.M. Woodward, S.D. Colson, W.A. Chupka and M.G. White, J. Phys. Chem. 90 (1986) 274;
W.A. Chupka, S.D. Colson, M.S. Seaver and A.M. Woodward, Chem. Phys. Letters 95 (1983) 171.
[7] J.A. Syage and J.E. Wessel, J. Chem. Phys. 87 (1987) 3313.
[8] K. Walter, R. Weinkauf, U. Boesl and E.W. Schlag, J. Chem. Phys. 89 (1988) 1914;
R. Weinkauf, K. Walter, U. Boesl and E.W. Schlag, Chem. Phys. Letters 141 (1987) 267.
[9] X. Ripoche, I. Dimicoli, J. Le Calvé, F. Piuzzi and R. Botter, Chem. Phys. 124 (1988) 305.
[10] D. Klapstein, S. Leutwyler and J.P. Maier, Chem. Phys. Letters 84 (1981) 534.
[11] A. Carrington and R.P. Tuckett, Chem. Phys. Letters 74 (1980) 19;
F.J. Grieman, A. McIlroy and J. Perkins, J. Chem. Phys. 84 (1986) 2481.
[12] J.A. Syage, J. Phys. Chem. 93 (1989) 170;
J.A. Syage, J.E. Pollard and R.B. Cohen, Appl. Opt. 26 (1987) 3516.

[13] J.A. Syage, Chem. Phys. Letters 143 (1988) 19.
[14] J.E. Pollard and R.B. Cohen, Rev. Sci. Instr. 58 (1987) 32.
[15] J.A. Syage, to be submitted for publication.
[16] W.C. Wiley and I.H. McLaren, Rev. Sci. Instr. 26 (1955) 1150.
[17] S.P. Goss, D.C. McGilvery, J.D. Morrison and D.L. Smith, J. Chem. Phys. 75 (1981) 1820;
D.C. McGilvery and J.D. Morrison, J. Chem. Phys. 67 (1977) 368.
[18] P.J. Dagdigian and J.P. Doering, J. Chem. Phys. 78 (1983) 1846.
[19] H. Helvajian, B.M. Dekoven and A.P. Baronavski, Chem. Phys. 90 (1984) 175;
B.M. DeKoven, D.H. Levy, H.H. Harris, B.R. Zegarski and T.A. Miller, J. Chem. Phys. 74 (1981) 5659.
[20] E.P. Muntz, Phys. Fluid 5 (1962) 80.
[21] J.W. Rabalais, Principles of ultraviolet photoelectron spectroscopy (Wiley, New York, 1977);
K. Kimura and S. Katsumata, HeI photoelectron spectra of organic compounds (Hokkosya Saika, Sapporo, 1978).
[22] J.B. Coon, R.E. DeWames and C.M. Loyd, J. Mol. Spectry. 8 (1962) 285;
F. Ansbacher, Z. Naturforsch. A 14 (1959) 889.